

1
2
3
4
5 **Sex-linked gene traffic underlies the acquisition of sexually dimorphic UV color**
6 **vision in *Heliconius* butterflies**

7
8
9 Mahul Chakraborty¹, Angelica Guadalupe Lara¹, Andrew Dang¹, Kyle J. McCulloch^{1,2},
10 Dylan Rainbow¹, David Carter³, Luna Thanh Ngo¹, Edwin Solares¹, Iskander Said⁴,
11 Russ Corbett-Detig⁴, Lawrence E. Gilbert⁵, J.J. Emerson^{1*}, Adriana D. Briscoe^{1*}

12
13
14
15
16
17 Affiliations:

18
19 ¹Department of Ecology and Evolutionary Biology, University of California, Irvine, CA
20 92697

21 ²Department of Ecology, Evolution and Behavior, University of Minnesota, St. Paul, MN
22 55108

23 ³Department of Molecular, Cell and Systems Biology, University of California, Riverside,
24 CA 92521

25 ⁴Department of Biomolecular Engineering and Genomics Institute, University of
26 California, Santa Cruz, CA 95064

27 ⁵Department of Integrative Biology, University of Texas, Austin, TX 78712

28
29 *Co-corresponding authors: abriscoe@uci.edu and jje@uci.edu

30

32 **Abstract**

33 Butterflies have photoreceptor cells that are sensitive to the ultraviolet part of the spectrum
34 due to *ultraviolet-sensitive rhodopsin (UVRh)*, a gene that has been duplicated in the *Heliconius*
35 genus. In individuals expressing UVRh1 and UVRh2, electrophysiological and behavioral studies
36 demonstrate that these opsin proteins enable discrimination of UV wavelengths. This
37 behavioral trait varies between species, being absent in *H. melpomene* and limited to females in
38 *H. erato*. To identify the evolutionary origins of this trait, we first examined UV color vision in *H.*
39 *charithonia*, a species related to *H. erato* in the *sara/sapho* group. We found that this species
40 also has sexually dimorphic UV color vision. To identify the genetic basis of this trait, we built a
41 reference-grade genome assembly of *H. charithonia*. We discovered that one duplicate, *UVRh1*,
42 is present on the W chromosome, making it obligately female-specific. We employed gDNA PCR
43 assays of *UVRh1* across the *Heliconius* genus. In species with sexually dimorphic *UVRh1* mRNA
44 expression, *UVRh1* gDNA is absent in males, whereas in species with sexually monomorphic
45 *UVRh1* mRNA expression, *UVRh1* gDNA is found in both sexes. The presence or absence of male
46 *UVRh1* expression across the *Heliconius* phylogeny supports a model where sexual dimorphism
47 was acquired early via movement of a gene duplication to the W-chromosome. We used
48 CRISPR-Cas9 to engineer a deletion in the *UVRh1* locus in female *H. charithonia* and use
49 immunohistochemistry to show that *UVRh1* protein expression is absent in mutant tissue,
50 similar to that of males. Our results show that a rare behavioral phenotype, sex-specific UV
51 color vision, was acquired via sex chromosome gene traffic of a duplicated UV rhodopsin.

52 The acquisition of novel sexually dimorphic traits poses an evolutionary puzzle: how
53 does a new trait arise and how does it become sex-limited? The persistence of sexual
54 dimorphism over evolutionary timescales implies that optimal phenotypes for such traits differ
55 between sexes. Discovering the molecular events leading to different phenotypic outcomes is
56 crucial to understanding the evolutionary mechanisms that resolve such sexually-mediated
57 tradeoffs (Rice 1984; Fry 2010). Candidate mechanisms include: the “pleiotropy-mechanism”
58 (PM) whereby the sex-limitation and the new trait arise simultaneously, avoiding a tradeoff;
59 and the “modifier-mechanism” (MM), whereby a new monomorphic trait arises first, followed
60 by the acquisition of modifiers that restore the ancestral state in one sex, thereby resolving the
61 tradeoff (Turner 1978; Rice 1984). The visual system offers one useful model for understanding
62 this process. The genetics and physiology of vision is well-understood for a number of animals,
63 and many instances of sexual dimorphism in the visual system, specifically in the expression of
64 opsins or photostable filtering pigments in insects, have been documented (Arikawa et al. 2005;
65 Sison-Mangus et al. 2006; Ogawa et al. 2012; Perry and Desplan 2016; McCulloch et al. 2017;
66 Liénard et al. 2021). Furthermore, sexual dimorphism for color vision behavior is observed in
67 both New World monkeys (Jacobs 1998) and in the butterfly genus *Heliconius* (Finkbeiner and
68 Briscoe 2021).

69 In animal vision, distinct photoreceptor cell subtypes can be sensitive to different
70 wavelengths of light. Variation in color sensitivity is primarily conferred by differences in the
71 rhodopsin pigments—opsin proteins together with a chromophore—that absorb light. The
72 integration of neural signals from different photoreceptor cells leads to color vision. In the
73 genus *Heliconius*, there are four opsin genes, which encode a green wavelength-absorbing
74 (LWRh), a blue wavelength-absorbing (BRh), and two ultraviolet wavelength-absorbing (UVRh1
75 and UVRh2) rhodopsins. The two UV rhodopsins are the consequence of a recent gene
76 duplication that occurred ~18.5 million years ago in the ancestor of all *Heliconius* butterflies
77 (Briscoe et al. 2010; Kozak et al. 2015). Individuals expressing both UVRh1 and UVRh2 opsins
78 can have at least two distinct ultraviolet-sensitive photoreceptor cell types, suggesting that
79 these individuals can distinguish different UV wavelengths. Indeed, intracellular recordings have
80 demonstrated different spectral sensitivities for two UV cell types in *H. erato* females

81 (McCulloch et al. 2016). Behavioral analysis has further shown that female *H. erato* butterflies
82 can distinguish different UV wavelengths (Finkbeiner and Briscoe 2021). On the other hand, *H.*
83 *melpomene* lacks this type of UV photoreceptor dimorphism and UV color vision behavior
84 (Finkbeiner and Briscoe 2021; McCulloch et al. 2022). Despite extensive genomic work in the
85 *Heliconius* genus, including a reference genome for *H. melpomene* (Davey et al. 2016), the
86 *erato/sara/sapho* clade lacks a genome assembly placing *UVRh1* on its chromosome (Lewis et
87 al. 2016), which is crucial to understanding the evolution of sexually dimorphic UV color vision.

88 To uncover the path evolution followed in acquiring divergent UV color vision
89 phenotypes between the *erato/sara/sapho* and *doris/melpomene* clades (Fig. 1A), we needed
90 to document the location, structure, and genomic context of both *UVRh* duplicates in
91 representatives of both clades. To accomplish this for the *erato/sara/sapho* clade, we built a
92 reference-quality genome assembly for *H. charithonia*—a species exhibiting differences in the
93 flower types visited by males and females (Mendoza-Cuenca and Macías-Ordóñez 2005)—to
94 compare against the existing high-quality draft genome of *H. melpomene* (Davey et al. 2016).
95 We used long read sequencing and RNA-seq data to create and annotate a highly contiguous,
96 complete, and accurate reference-grade genome assembly (Figs. S1-4). In addition to
97 recovering 99% of Lepidopteran Benchmarking Universal Single Copy Orthologs (BUSCO) in the
98 assembly (Manni et al. 2021), 50% of the sequence is represented by contigs 16.4 Mb and
99 longer (i.e. contig N50 = 16.4 Mb). Upon scaffolding with Hi-C, we attained sequences that span
100 chromosomes nearly end-to-end (scaffold N50 = 17 Mb). Moreover, we also recovered a large
101 scaffold representing the W-chromosome (Fig 1B-E). To our surprise, *UVRh1* is located on the W
102 scaffold, in contrast with *H. melpomene*, in which both *UVRh* duplicates are autosomal (Fig. 2A-
103 E)(*Heliconius* Genome Consortium 2012). In the outgroup species *Eueides isabella* and *Dryas*
104 *iulia*, a single *UVRh* gene occupies the genomic location corresponding to *Heliconius UVRh2* (Fig.
105 2E).

106 The descendant of this ancestral locus resides on chromosome 12 in *E. isabella*, which is
107 syntenic with the location of *UVRh2* on chromosome 7 in *H. melpomene*, while *UVRh1* is
108 present on chromosome 17 in *H. melpomene* (Fig. 2A,E). To determine the sex linkage of *UVRh1*
109 in representative species across the genus, we designed gDNA PCR assays targeting *UVRh1* in

110 10 species, five of which show sexually dimorphic UVRh1 protein expression (McCulloch et al.
111 2017). We successfully amplified and sequenced PCR products specific to *UVRh1* for all species
112 (Fig. 3, S5, S6). For species in the *doris/melpomene* clades, we recovered *UVRh1* amplicons in
113 both sexes. However, for species in the *erato/sara/sapho* clades, the *UVRh1* amplicons were
114 limited to females. In all cases, positive control amplicons were present in both sexes (Fig. 3B).
115 Using a phylogeny of 20 species and a maximum likelihood approach, we inferred that absence
116 of *UVRh1* in males was the likely ancestral state of the *erato/sara/sapho* clade. However, we
117 were unable to infer whether or not *UVRh1* was absent in males at the base of the genus
118 *Heliconius* because the *erato/sara/sapho* and the *doris/melpomene* clades are sister groups
119 (Fig. S8). Either *UVRh* was first duplicated onto the W-chromosome in the *Heliconius* common
120 ancestor, limiting *UVRh1* to females, or *UVRh* was first duplicated onto an autosome. Under the
121 first scenario, a translocation in the common ancestor of the *doris/melpomene* clades then
122 moved *UVRh1* from the W to the homolog of chromosome 17 in *H. melpomene*, initiating
123 autosomal linkage. Under the second scenario, a translocation in the common ancestor of the
124 *erato/sara/sapho* clades then moved *UVRh1* from the homolog of chromosome 17 to the W.

125 To establish that the *H. charithonia* gene we annotate as *UVRh1* encodes the UVRh1
126 protein in female photoreceptor cells, we knocked out the *UVRh1* gene in the adult eye. To
127 achieve this via CRISPR-mediated deletion, we designed two guide RNAs targeting the 2nd and
128 3rd exons of *UVRh1*. We co-injected Cas9 and the gRNAs into 0-1 hour embryos and reared the
129 survivors into adulthood. To visualize the locations of the short-wavelength opsins, the eyes
130 were fixed and stained with anti-UVRh1, -UVRh2, and -BRh opsin antibodies. Adult CRISPR-
131 edited female eye tissue exhibited mosaicism for two tissue types: female tissue with UVRh1,
132 UVRh2, and BRh opsin-expressing photoreceptors, and male-like tissue containing only UVRh2
133 and BRh opsin-expressing photoreceptors (Fig. 4, Fig. S7J, S9).

134 Finally, we conducted behavioral trials to confirm that the expression of UVRh1 and
135 UVRh2 in photoreceptor cells in female *H. charithonia* eyes confers the ability of adults to
136 discriminate between different wavelengths of ultraviolet light. Adult male and female
137 butterflies were trained to associate a sugar reward with 390 nm UV light following the
138 protocol of Finkbeiner and Briscoe (2021). After training, adults were then given a choice

139 between two UV lights: a rewarded light (390 nm), and an unrewarded light (380 nm)(Fig. S10).
140 Individuals that flew to a light source were scored as selecting that light source. Females
141 exhibited a strong and significant preference for 390 nm, the rewarded light, regardless of the
142 relative intensity of the stimuli (z value=2.739, p-value=0.01) (Fig. 4E, Tables S2, S3), indicating
143 that females have UV color vision. In contrast, males exhibited a preference for the brighter
144 light source, correctly and significantly selecting the trained wavelength only when it was
145 brightest (z value=2.739, p-value=0.01)(Fig. 4E, S8, Tables S2, S3), an indication of positive UV
146 phototaxis but not UV color vision.

147 Here we show that gene traffic from an autosome to the W chromosome is the genetic
148 mechanism behind the acquisition of sex-specific UV opsin expression in *Heliconius*. Relocation
149 of the duplicate gene *UVRh1* to the W chromosome in the *erato/sara/sapho* clades leads to its
150 absence in males, making it female-specific. A requirement for color vision is the specialization
151 of photoreceptor cells to be sensitive to different wavelengths of light. Previous studies showed
152 that rapid molecular divergence of *UVRh2* compared to *UVRh1* has led to extensive amino acid
153 variation between the two duplicates (Briscoe et al. 2010), likely resulting in spectral tuning of
154 *UVRh2* associated with functional divergence in photoreceptor spectral sensitivity (McCulloch
155 et al. 2016; McCulloch et al. 2022). Regardless of the specific path taken in UV opsin evolution,
156 what is clear is that the duplication of the ancestral UV rhodopsin was followed by acquisition
157 both of a novel expression pattern in females and of a novel protein function.

158 To classify the path followed in the molecular evolution of novel sexually dimorphic UV
159 color vision, we consider the two previous models—the pleiotropy mechanism (PM) (Rice 1984)
160 and the modifier model (MM) (Rice 1984)—and propose a third: partitioning-first (PF) whereby
161 the genetic basis of the trait is first partitioned by sex, followed by a shift in the phenotype. In
162 cases of duplication of genes like opsins, each copy can in principle correspond to
163 independently mutable instances of the trait. This has two relevant consequences. First, gene
164 duplication may avoid sexually antagonistic fitness tradeoffs, as independent fitness optima can
165 be achieved simultaneously for each copy (Connallon and Clark 2011; Chakraborty and Fry
166 2015). Second, duplication permits sex-biased partitioning to precede the shift of a trait fitness
167 value. For example, retrogenes successfully escaping the X chromosome in mammals

168 immediately cease existing in an environment subject to meiotic X-inactivation, a process
169 specific to male biology (Long and Emerson 2017). In the evolution of UV color vision, the path
170 to the phenotype shift and the sex-specificity did not happen simultaneously so the pleiotropy
171 model is a poor fit. Since most of the rapid amino acid evolution of UVRh2 occurred in a
172 common ancestor of *Heliconius* with two *UVRh* genes, the order of the mutations will
173 determine whether the spectral sensitivity shift (MM) or sexually dimorphic partitioning (PF)
174 happened first. Finer genome-level sampling of *Heliconius* will facilitate more refined
175 phylogenetic hypotheses (Turner 1976), potentially resolving the specific evolutionary sequence
176 of events. It is intriguing too, that the *erato/sara/sapho* clade is united not only by the loss of
177 *UVRh1* in males but also in pupal mating and its associated morphology (e.g. the absence of
178 signa in female bursa copulatrix)(Penz 1999) and behavior (e.g. the ability of males to
179 discriminate the sex of pupae)(Estrada et al. 2010). These traits may be intriguing candidates
180 for driving differences in vision between the two major *Heliconius* subclades characterized
181 here.

182 X-linked opsin gene expression has been shown to underlie sexual dimorphism of red-
183 green color vision in New World monkeys (Hunt et al. 1998). However an important difference
184 exists between the red-green color vision dimorphism of NW primates, which is based on a
185 single-gene allelic system, and the UV color vision dimorphism in *Heliconius* described here.
186 Elucidating the transcriptional mechanisms that control UV opsin expression will shed light into
187 the processes regulating sex-specific gene expression, and the identification of associated
188 downstream neural circuitry changes will provide insights into the evolution of behavioral
189 differences between the sexes. In conclusion we show that an extreme form of female-limited
190 UV color vision behavior in butterflies has evolved via gene duplication followed by sex
191 chromosome translocation and that this finding reveals how novel sex-specific complex traits
192 can arise in a short evolutionary time.

193

194 **Acknowledgements**

195 We thank Javier Rodarte, Zachary Johnson, Aline Rangel Olguin, Yuan Tao, Furong Yuan, JP
196 Lawrence, Matthew Aardema, Peter Andolfatto and Stephannie Seng for technical assistance
197 and UCI's Optical Biology Core for microscopy access. This work was funded in part by NSF grant
198 IOS-1656260 to A.D.B, NIH grants R01GM123303-1 to J.J.E. and K99GM129411 to M.C., and
199 through grants CA-62203 and GM-076516 supporting UCI's Optical Biology Core Facility.

200 **Methods**

201 **Butterfly samples**

202 A single pair mating of *H. charithonia* was generated in the greenhouse at the University of
203 Texas, Austin in October 2017. From this mating, a single adult female F1 specimen was used in
204 the generation of Hi-C data. Extraction of high molecular weight from other F1 adults from this
205 mating did not yield DNA of sufficiently high quality so in March 2018, a female pupa
206 descended from the UT colony was used to generate the PacBio data. Two other male and
207 female individuals from the same source were used for Illumina DNA short-read sequencing.
208 Embryos used for CRISPR injection were collected from mated females descended from pupae
209 sourced from the Costa Rica Entomological Supply. Locality information for specimens used in
210 PCR and behavioral experiments are given in Table S4.

211 **DNA extraction and Sequencing**

212 High molecular weight genomic DNA was extracted from a single *H. charithonia* female pupa
213 following established protocols (Chakraborty et al. 2016). Briefly, the pupa was cut open from
214 the posterior end using a razor blade and the soft tissue was squeezed out using a
215 homogenizer. The tissue was homogenized in buffer G2 of Qiagen Blood and Cell Culture Tissue
216 Kit and rest of the DNA extraction was carried out as described in Chakraborty et al. (2016).
217 DNA was sheared with 10 plunges of 21 gauge blunt-end needle followed by 10 plunges of 24
218 gauge blunt-end needle. The sheared DNA was size selected on Blue Pippin using 20 kb
219 minimum cut-off length and a library was created from this size selected DNA. The library was

220 sequenced with 33 SMRTcells on the Pacific Biosciences RS II platform, producing a total of 49.5
221 Gbp sequences (50% of the reads are 18.3 kbp or longer).

222 **Genome assembly**

223 We generated two initial assemblies, one with Falcon and the other with Canu (v1.6)(Koren et
224 al. 2017). The primary Falcon assembly was merged with the canu assembly using quickmerge
225 (Chakraborty et al. 2016), wherein the Canu assembly served as the query. Falcon is a diploid-
226 aware assembler so it can assemble through heterozygous genomic regions that are recalcitrant
227 to Canu. Thus, gaps in the Canu assembly were filled by sequences from the Falcon assembly.
228 This assembly was polished twice with Arrow from SMRT Analysis (v5.1.0) (Chin et al. 2013) and
229 then twice with Pilon (Walker et al. 2014) using 1,203 million 150 bp PE reads (Table S4). The
230 presence of two haplotypes in the raw data may cause the polished assembly to generate
231 redundant sequences if contigs representing alternate haplotypes (i.e. haplotigs) are not
232 identified. To identify alternate haplotigs, we aligned the assembly to itself using Nucmer (--
233 maxmatch --no-simplify) (Marçais et al. 2018) and identified contigs that were completely
234 embedded within bigger contigs. The sequences in the resulting assembly were marked as
235 either “alt_hap” or “primary” based on whether they were embedded in another contig or not,
236 respectively. While this approach can potentially be confounded by incorrect assembly of
237 repetitive sequences (Phillippy et al. 2008) and aggressively purging alternative haplotigs may
238 remove real duplicate mutations, such adverse outcomes in high quality long-read-based
239 assembly like the *H. charithonia* assembly reported here are rare relative to misassemblies that
240 generate contigs with redundant sequence information (Roach et al. 2018; Guan et al. 2020;
241 Solares et al. 2021). Even so, the placement of rare redundant contigs representing real
242 duplicates is uncertain, diminishing the value in retaining them.

243 **Microbial decontamination**

244 To decontaminate the microbial sequences from the polished contigs, taxonomic groups were
245 assigned to each contig using Kraken2 (Wood et al. 2019). We identified 4 contigs that were
246 derived from non-butterfly sources (three bacterial and one from nematode). We removed
247 these sequences from the assembly prior to scaffolding and downstream analysis.

248 **Scaffolding**

249 Hi-C libraries were constructed from a *H. charithonia* female adult whole body. The library was
250 sequenced with PE 75 bp reads on Illumina HiSeq 2500, generating 132,937,739 reads. The
251 reads were mapped to the primary polished and decontaminated assembly using Juicer
252 (Durand et al. 2016) with the default parameters. The contact density map was created from
253 the alignment using the Juicer pipeline and the primary contigs were scaffolded using the Hi-C
254 interaction map following the 3D-DNA pipeline. Among the 70 contigs identified as putatively
255 W-linked (see below), 60 contigs showed Hi-C contacts between them and were joined in a
256 scaffold in Juicebox, following the order suggested by 3D-DNA (Dudchenko et al. 2017). The
257 final assembly contained 21 major scaffolds representing the 19 autosomes, a Z chromosome ,
258 and a W chromosome.

259 **Automated gene annotation**

260 We generated RNA-seq reads from mRNA extracted from antennae, mouthparts and legs of
261 adult *H. charithonia* males and females. Together with previously published RNA-seq data from
262 heads (Catalan et al. 2019), we aligned the reads to the assembly using Hisat2 (Kim et al. 2019).
263 The transcripts were annotated and merged using StringTie (Pertea et al. 2016). We first ran
264 Braker2 (Brůna et al. 2021) to generate a draft annotation based on the *H. charithonia* RNA-seq
265 evidence and protein sequences from *H. melpomene melpomene*. The *H. charithonia* Braker2
266 annotation, the *H. melpomene* protein and mRNA sequences (Davey et al. 2016), and the *H.*
267 *charithonia* merged stringtie transcript sequences were used as evidence in Maker2 for gene
268 model prediction (Holt and Yandell 2011). The consensus repeat sequences from
269 Repeatmodeler (see below) was used as the repeat library in Maker2. Maker2 was run in three
270 rounds: in the first run annotation was performed using EST and protein hints, in the second
271 run, Augustus and SNAP predictions were added, and in the third step Genemark predictions
272 were added. The Augustus training was performed in Braker2 and the SNAP prediction was
273 performed using the gene models from the first run of Maker.

274

275 **Manual gene annotation**

276 Custom BLAST databases of *H. charithonia* mRNA transcripts were generated from *de novo*
277 (Trinity) and genome-guided transcriptome assemblies of eye, brain, antennae, mouthparts and
278 leg RNA-Seq from adult butterflies. Amino acid sequences for chemosensory proteins (CSPs),
279 odorant binding proteins (OBPs) and olfactory receptors (ORs) identified in *Heliconius* Genome
280 Consortium et al. (*Heliconius* Genome Consortium 2012) and Briscoe et al. (Briscoe et al. 2013)
281 were used as tBLASTN query sequences against this transcriptome in order to identify *H.*
282 *charithonia* orthologs. Curated OBP, CSP, and OR protein sequences were aligned in MEGA X
283 using MUSCLE. These alignments were visually inspected and manually adjusted. Maximum
284 likelihood trees were estimated in PhyML (Guindon et al. 2010) from the nucleotides using 500
285 bootstrap replicates and the best-fit substitution models as identified by SMS (Lefort et al.
286 2017). The Akaike Information Criterion was used as the selection criterion.

287 **Repeat annotation**

288 We created a custom repeat library using EDTA (Ou et al. 2019) and Repeatmodeler (Flynn et al.
289 2020). LTR retrotransposons and DNA elements were detected using the EDTA pipeline because
290 EDTA is more accurate at finding intact elements than Repeatmodeler. In EDTA, we used the *H.*
291 *charithonia* protein sequences from the final Maker run for filtering out predicted TEs that
292 overlapped protein coding sequences. Because EDTA does not annotate non-LTR
293 retrotransposons, the non-LTR elements were identified using Repeatmodeler and added to the
294 repeat library.

295 **Identification of W-linked sequences**

296 To identify the W-linked sequences, male and female Illumina paired-end genomic DNA reads
297 were aligned to the polished and decontaminated contig assembly using Bowtie2
298 (v2.2.7)(Langmead and Salzberg 2012). Alignments were sorted and male and female Illumina
299 read coverage (Table S4) of each contig was measured using Bedtools (bedtools coverage -
300 mean)(Quinlan and Hall 2010) and contigs showing at least 2-fold higher coverage for female
301 reads than male reads were designated as putative W-linked contigs. The contigs showing >2
302 fold male-to-female coverage ratio were assigned as the candidate Z contigs. This Z

303 chromosome candidate mapped to the *H. erato* Z chromosome, suggesting that the coverage
304 based sex-chromosome assignment identified sex-linked chromosomes correctly (Fig. S4).
305 Contigs showing enrichment of female k-mers were marked as candidates for W-linked
306 sequences. Finally, we mapped the RNA-seq reads from males and females to repeat-masked
307 putative W-linked sequences and compared the male vs. female transcript abundance in the
308 putative W-linked genes.

309 ***UVRh1* PCR amplification**

310 To examine the sex-linkage of *UVRh1* in 10 *Heliconius* species, genomic DNA was extracted from
311 the dissected thorax of single adult male and female butterflies from each species using
312 Monarch Genomic DNA Purification Kit (New England Biolabs) following the manufacturer's
313 protocol, except we added 10 μ L of proteinase K to each sample. To amplify *UVRh1* genomic
314 sequence, we used the primer pairs 5' CGCTACAGTCTTGCAAGCTAC 3' and 5'
315 ATATTCTACAGTGGAAATCGTAAAA 3'. For all amplifications using the *UVRh1*-specific primers,
316 we used Phusion HF Polymerase (New England Biolabs) and annealing temperatures (Tm) of
317 60°C and 58°C, respectively. To rule out missing amplicons due to PCR failure in the fresh
318 genomic DNA samples, we used the forward primer (ef44) 5' GCGGARCGYGARCGTGGTATYAC 3'
319 and reverse primer (efrcM4) 5' ACAGCVACKGYTGYCTCATRTC 3' to amplify the housekeeping
320 gene *EF1a*. The purified *UVRh1* amplicons were cloned into the minT vector using the PCR
321 cloning kit and following the manufacturer's protocol (NEB). The cloned amplicons were
322 sequenced by Retrogen Inc. using the NEB-F, NEB-R primers supplied by the manufacturer.
323

324 **Ancestral state reconstruction**

325 Presence or absence of *UVRh1* mRNA or protein expression in adult male *Heliconius* eyes was
326 determined based on RNA-seq data of McCulloch et al. (2017), reproduced in Table S1 and
327 and/or immunohistochemistry shown in Fig. S7. Characters were mapped on a trimmed
328 *Heliconius* species phylogeny (Kozak et al. 2015) using Mesquite v.3.10. Ancestral state
329 likelihood analysis was performed in Mesquite using binary character states.

330 ***UVRh1* knockout using CRISPR**

331 To knock out *UVRh1* using CRISPR (Jinek et al. 2012), we designed two gRNAs (5'
332 GGAGTACAGCAACGCTAGTG 3', 5' GGTTTGCTACAGGTGCTT 3') that target the second and
333 third exons of *UVRh1*, respectively. The gRNAs were synthesized (Synthego) and were
334 combined with Cas9 (EnGen® Spy Cas9 NLS, New England Biolabs) at concentrations 160 ng/uL
335 and 240 ng/uL, respectively.

336 Embryos were collected by giving fresh young *Passiflora biflora* shoots to adults for one
337 hour and the collected embryos were soaked in 5% benzylkonium chloride solution (Millipore
338 Sigma) for 5 minutes for disinfection. The gRNA-Cas9 mixture was incubated at room
339 temperature for 10 minutes for formation of ribonucleoprotein complex and was injected into
340 0-1.5h embryos attached to a double-sided tape on a glass slide. Injected embryos were kept
341 inside a petri dish for 4 days at room temperature with moistened Kimwipes to maintain
342 humidity. Eggs hatched after ~4 days and the ~4 days old caterpillars were transferred to a *P.*
343 *biflora* inside a mesh cage. Adults eclosed after approximately four weeks and were genotyped
344 for the CRISPR mediated deletion using PCR.

345 To screen adults for the CRISPR-mediated deletion, we extracted genomic DNA from a
346 hind leg of each adult using Monarch Genomic DNA Purification Kit (New England Biolabs) and
347 amplified the DNA using a *UVRh1*-specific primer pair (5' CAAGCATTGTCATTGATGCA 3', 5'
348 GAAACGCAAAACTACAACGTT 3') that produced a 708 bp and 390 bp amplicons for uncut and
349 cut *UVRh1* genomic sequences, respectively.

350

351 **Immunohistochemistry of adult eyes**

352 Methods were adapted from previous studies (Hsiao et al. 2012; Perry et al. 2016;
353 McCulloch et al. 2017). Dissected *H. charithonia* eyes were fixed in 4% paraformaldehyde (in 1x
354 PBS) for one hour at room temperature with one hour baths at room temperature in increasing
355 concentrations of sucrose (10, 20, and 30%) afterwards. The corneal lens was then excised
356 from each eye and the eyes were embedded in blocks of gelatin-albumin. The blocks were then
357 fixed in 4% formalin (in 1x PBS) for six hours and a VF-310-0Z Compresstome (Precisionary) was

358 used to cut 50 μ m slices. Tissue slices were blocked for one hour in 10% (v/v) normal goat
359 serum and normal donkey serum and 0.3% Triton X-100 (in 1X PBS). Tissues were incubated
360 with preadsorbed primary antibodies (1:15 guinea pig anti-UVRh1, 2:75 rabbit anti-UVRh2, and
361 1:15 chicken anti-BRh in blocking solution) overnight at 4°C. Tissues were washed 5X 15
362 minutes in 1x PBS and incubated overnight at 4°C with secondary antibodies (1:250 goat anti-
363 guinea pig AlexaFluor 633, 1:250 donkey anti-rabbit Cy3, and 1:250 goat anti-chicken AlexaFluor
364 488 in blocking solution). Afterwards, tissues were then washed 5x 15 minutes in PBST and then
365 mounted in 70% glycerol. Images were taken using a Zeiss LSM 900 Airyscan 2 confocal
366 microscope under a 20x/0.8NA dry objective in the UC Irvine Optical Core Facility, exported
367 using ZenBlue 3.5, and processed/pseudocolored using Fiji (Schindelin et al. 2012).

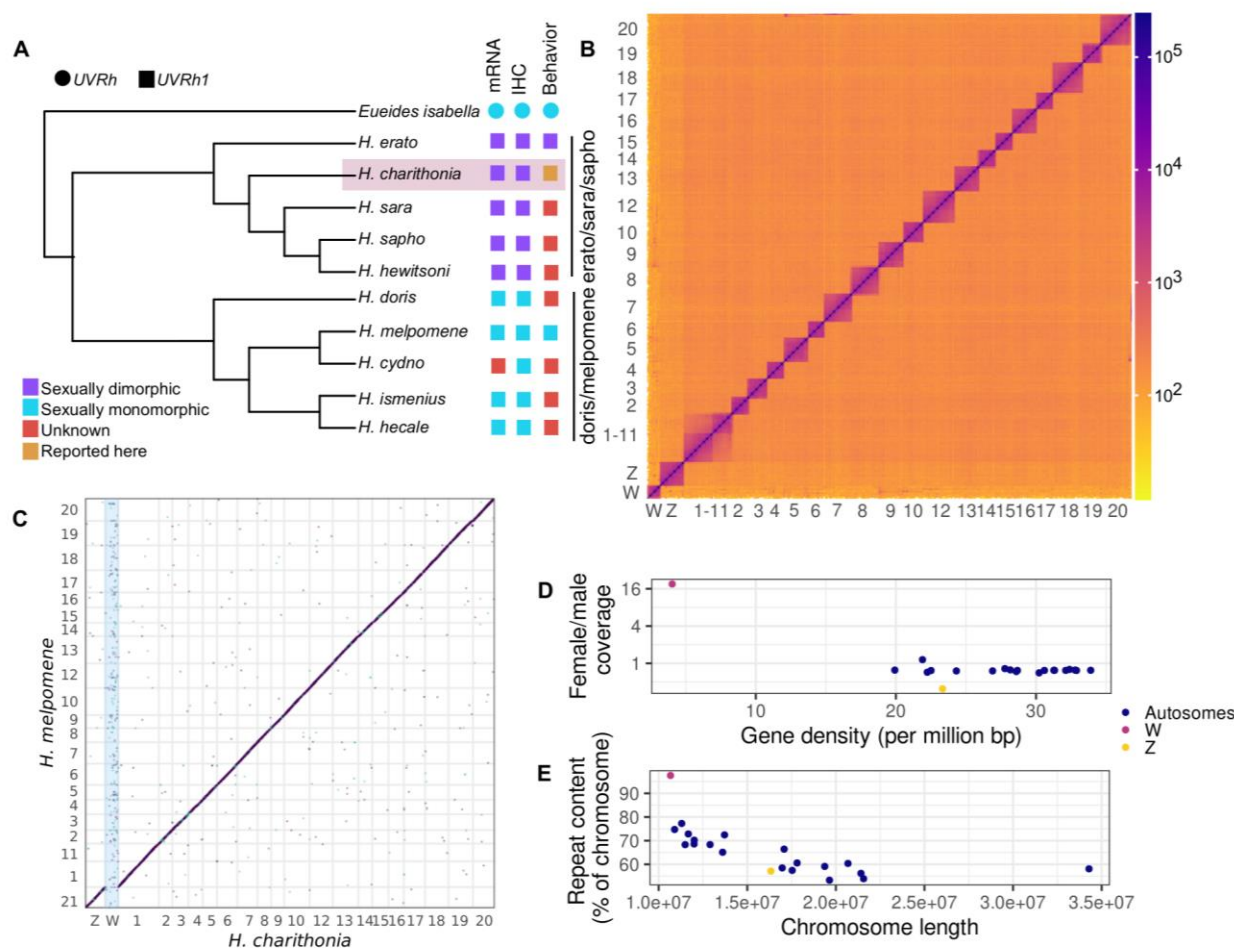
368

369 **Behavioral trials**

370 Both 390 nm and 380 nm 10 nm bandpass filtered lights were on during training at 1:1 intensity
371 but only 390 nm light was rewarded with 10% honey water supplemented with pollen (+) while
372 the unrewarded light had water (-). After training, both sexes (n=3 individual butterflies per sex)
373 were then tested for UV discrimination ability between 390 nm (+) and 380 nm (-) over three
374 different intensity combinations where the relative intensity of the rewarded:unrewarded lights
375 was 1:5, 1:1, or 5:1 (n=15 trials per intensity). During training and between training sessions,
376 the placement of the rewarded and unrewarded stimuli was randomly switched so that the
377 butterfly did not learn to associate the position of the light with a reward. The apparatus was
378 cleaned after each session with 70% isopropyl alcohol to remove chemical cues. After about 4–
379 5 days of training, butterflies were capable of independently flying toward the apparatus and
380 making a choice between the two light stimuli. Three different approximate ratios of the peak
381 physical intensities or absolute brightnesses of the rewarded/unrewarded stimuli were used:
382 0.02, 1.0 and 5.0 (or 1:5, 1:1, and 5:1)(Fig. S10). Butterflies first completed trials at an intensity
383 combination of 1:1 (15 choices each). Following this test they were given random choices
384 between intensities of 1:5 or 5:1 (rewarded:unrewarded) until they had completed 15 choices
385 with each intensity combination. The number of correct versus incorrect choices each butterfly

386 made at different intensity combinations was modeled using a general linear model with
387 Poisson distribution in R statistical software (version 4.1.1).

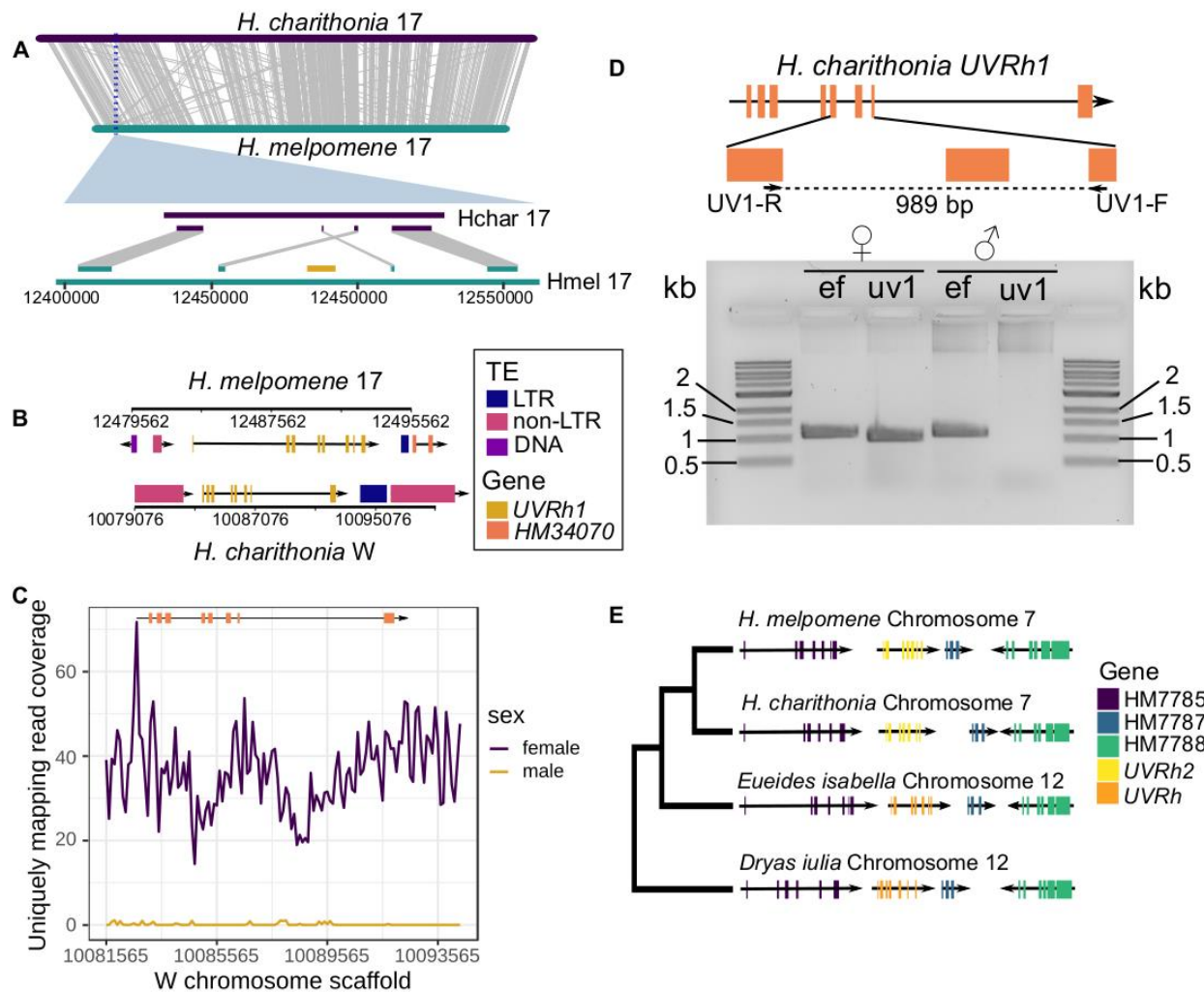
388 **Figures**



389

390 **Figure 1.** A *de novo* genome assembly of *Heliconius charithonia* and its phylogenetic
 391 relationship with species showing sexually monomorphic and dimorphic *UVRh1* expression. A) A
 392 cladogram showing the phylogenetic relationship among 10 *Heliconius* species, including *H.*
 393 *charithonia* and outgroup species *E. isabella*, based on Kozak et al. (2015). Five species from the
 394 *erato/sara/sapho* clades show sexually dimorphic expression of *UVRh1* mRNA and protein
 395 (immunohistochemistry or IHC) and female *H. erato* show UV color vision behavior. UV color
 396 discrimination in *H. charithonia* is reported in the present study. *UVRh1* expression in other
 397 species is either sexually monomorphic or unknown. B) A Hi-C contact density map of the *H.*
 398 *charithonia* genome assembly showing 21 chromosomes. Chromosome 1 is a fusion of two
 399 chromosomes. C) An alignment dot plot between the genome assemblies of *H. melpomene* and
 400 *H. charithonia*. As shown here, *H. charithonia* Chromosome 1 is a fusion of *H. melpomene*

401 Chromosomes 1 & 11 and the W scaffold has no corresponding sequence in the *H. melpomene*
402 assembly, which represents a male genome. D) Gene density and the ratio of female and male
403 short read coverage of 21 *H. charithonia* chromosomes. The W scaffold has very few protein
404 coding genes and virtually no unique sequence shared with a male genome. E) Relationship
405 between chromosome length and repeat content of *H. charithonia* chromosomes. The
406 chromosomes show a negative correlation between length and repeat content.
407



408

409 **Figure 2.** Genomic location of *UVRh1* and *UVRh2* in *Heliconius*. A) Alignment between *H.*
 410 *charithonia* and *H. melpomene* Chromosome 17 showing global synteny between the two
 411 chromosomes, although *UVRh1* is missing from *H. charithonia* Chromosome 17 . B) *UVRh1*
 412 cDNA maps to the W scaffold in *H. charithonia* and shares the same number of exons and
 413 introns as *H. melpomene* *UVRh1*. Presence of similar TE sequences on both sides of *UVRh1* in *H.*
 414 *melpomene* and *H. charithonia* indicates a possible role of TEs in translocation of *UVRh1*. C)
 415 Mapping coverage of uniquely mapping male and female Illumina paired end reads to the W
 416 scaffold region containing *UVRh1*. Virtually zero coverage of male reads supports the female
 417 linkage of *UVRh1*. D) Confirmation of W-linkage of *UVRh1* using PCR. A *UVRh1*-specific primer
 418 pair (uv1) amplifies only female *H. charithonia* gDNA but not male gDNA. The control primer
 419 *EF1a* (ef) amplifies both male and female gDNA. E) Genomic location of *UVRh2* in *H. melpomene*

420 and in *H. charithonia* and of *UVRh* in two outgroup species *Eueides isabella* and *Dryas iulia*
421 (Cicconardi et al. 2021; Lewis et al. 2021) along with three other genes in *H. melpomene*
422 reference genome release 2.5 (Davey et al. 2016). Conserved synteny of the genes suggest that
423 *UVRh2*, on *Heliconius* chromosome 7, retains the genomic location of ancestral single copy
424 *UVRh*, which is on *Eueides* chromosome 12.

425

426

427

428

429

430

431

432

433

434

435

436

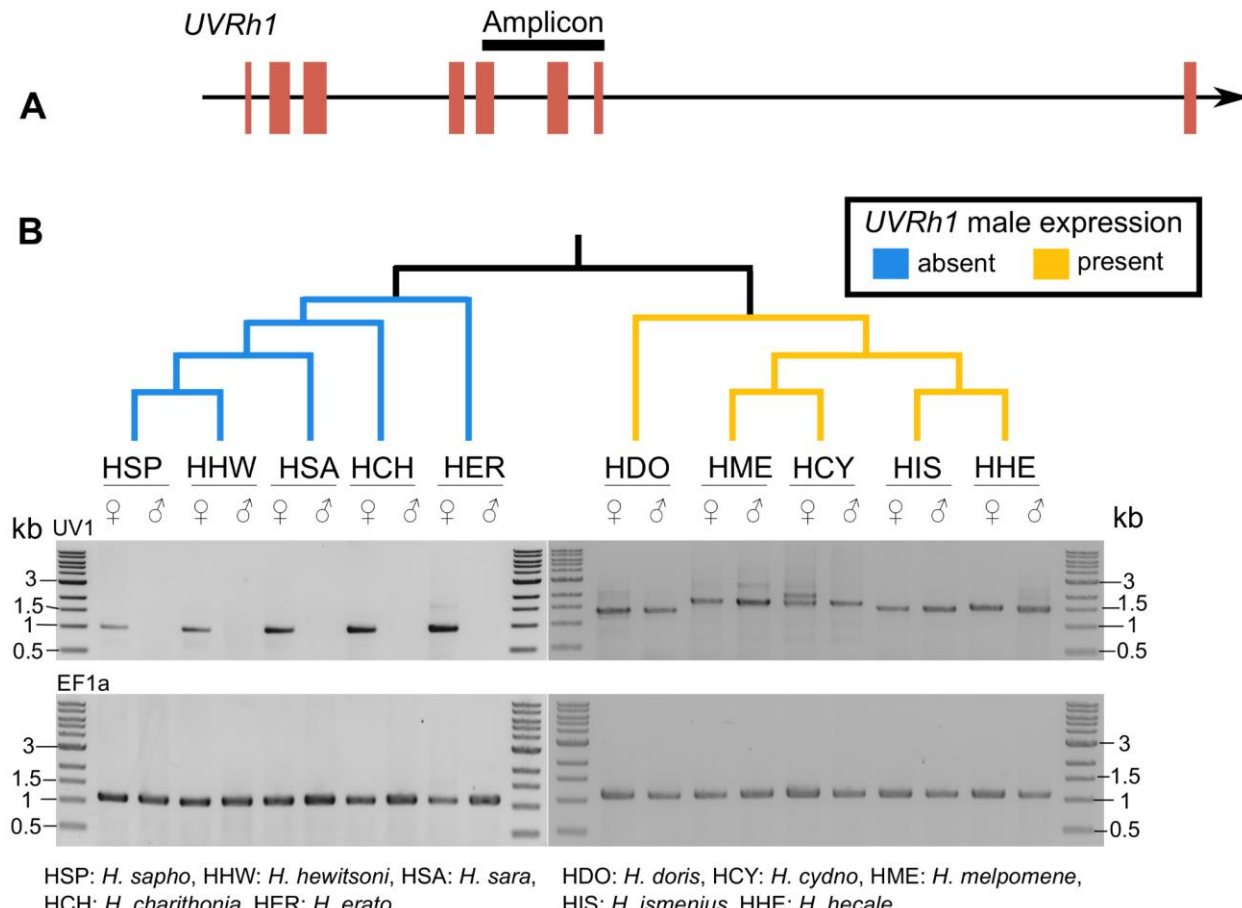
437

438

439

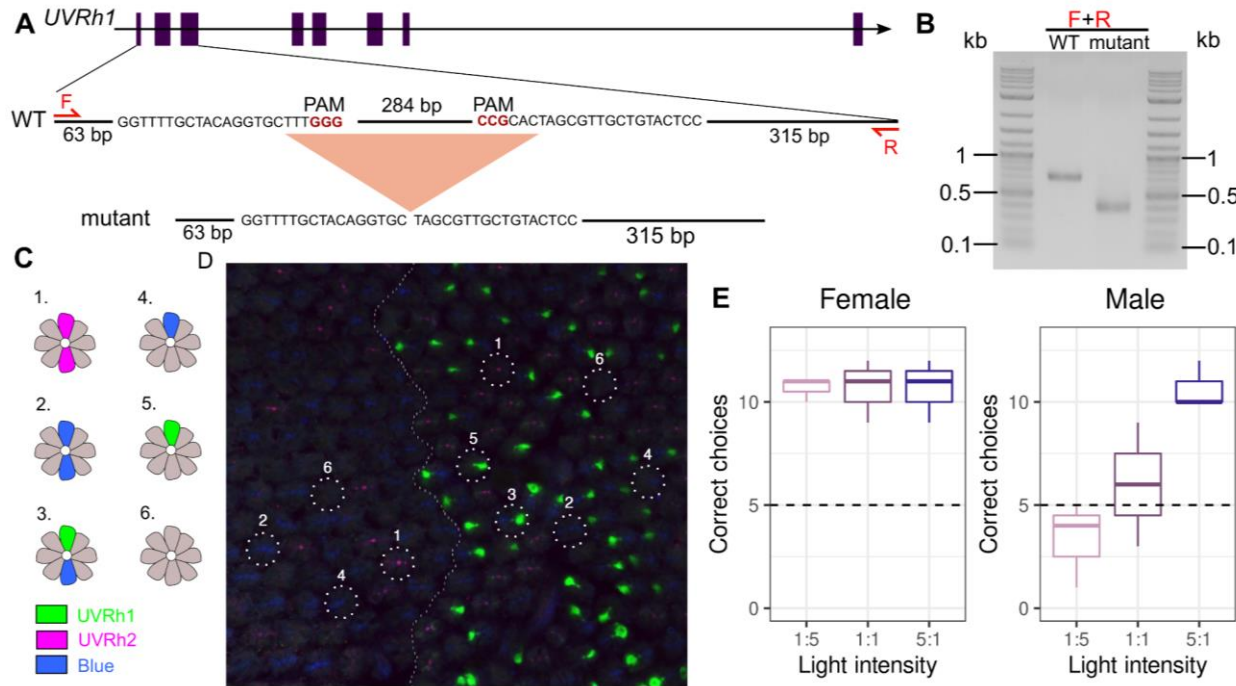
440

441



442 HSP: $H. sapho$, HHW: $H. hewitsoni$, HSA: $H. sara$, HDO: $H. doris$, HCY: $H. cydno$, HME: $H. melpomene$,
EF1a HCH: $H. charithonia$, HER: $H. erato$ HIS: $H. ismenius$, HHE: $H. hecale$

443 **Figure 3.** Determining *UVRh1* linkage across the genus *Heliconius* using gDNA PCR. A) Cartoon of
444 the relative length of the *UVRh1* amplicon used to determine sex-linkage of *UVRh1* in 10
445 *Heliconius* species. B) *UVRh1* PCR products from 10 *Heliconius* species, five of which show
446 sexually dimorphic *UVRh1* amplification. Only female DNA from the five species shown in blue
447 and both sexes in the five species shown in yellow produced the *UVRh1* amplicon. *H. cydno*
448 females produced an additional *UVRh1* PCR product that is absent in males (Fig. S5). The
449 cladogram on top of the gel is based on the published *Heliconius* phylogeny (Kozak et al. 2015).
450



451

452

453 **Figure 4.** Targeted CRISPR/Cas9 knockout of *UVRh1* in an adult *H. charithonia* female eye and
454 UV color vision behavioral trials. A) *UVRh1* gene model and sequence showing the location of a
455 296 bp deletion resulting from CRISPR/Cas 9 mutagenesis. B) PCR products of *UVRh1* genomic
456 region flanking the deletion. C) Cartoon: Wild-type *H. charithonia* female retinas have at least
457 six types of ommatidia based on opsin expression in the R1 and R2 photoreceptor cells: 1.
458 UVRh2/UVRh2, 2. BRh/BRh, 3. UVRh1/BRh, 4. BRh-LWRh/BRh, 5. UVRh1/LWRh-BRh, 6. LWRh-
459 BRh/LWRh-BRh (LWRh1 and BRh co-expression shown in Fig. S9). D) CRISPR targeted *UVRh1*
460 produces adult female retinas that lack UVRh1 protein in large domains (middle panel (left),
461 compared to wild-type, middle panel (right)). Knockout of *UVRh1* eliminates UVRh1 (green)
462 protein expression in ommatidial types 3 and 5 (left) while UVRh2 (magenta) ommatidial type 1
463 and BRh (blue) ommatidial types 2 and 4 are retained (left). E) Number of correct choices by *H.*
464 *charithonia* adult butterflies for the rewarded wavelength (+) when given a choice between 390
465 nm (+) and 380 nm (-) light under varying intensities. N=3 biological replicates per sex, N=15
466 choice trials per intensity. Females show a significant preference for the rewarded light over all
467 light intensities (p-value=0.01) while males only show a significant preference for the rewarded

468 light at the 5:1 intensity (p-value=0.01). Boxes represent upper and lower quartiles with
469 median; whiskers indicate 25th and 75th percentiles.

470 **References**

471 Arikawa K, Wakakuwa M, Qiu X, Kurasawa M, Stavenga DG. 2005. Sexual dimorphism of short-
472 wavelength photoreceptors in the small white butterfly, *Pieris rapae crucivora*. *J. Neurosci.*
473 25:5935–5942.

474 Briscoe AD, Bybee SM, Bernard GD, Yuan F, Sison-Mangus MP, Reed RD, Warren AD, Llorente-
475 Bousquets J, Chiao C-C. 2010. Positive selection of a duplicated UV-sensitive visual pigment
476 coincides with wing pigment evolution in *Heliconius* butterflies. *Proc. Natl. Acad. Sci. U. S.*
477 A. 107:3628–3633.

478 Briscoe AD, Macias-Muñoz A, Kozak KM, Walters JR, Yuan F, Jamie GA, Martin SH,
479 Dasmahapatra KK, Ferguson LC, Mallet J, et al. 2013. Female behaviour drives expression
480 and evolution of gustatory receptors in butterflies. *PLoS Genet.* 9:e1003620.

481 Brúna T, Hoff KJ, Lomsadze A, Stanke M, Borodovsky M. 2021. BRAKER2: automatic eukaryotic
482 genome annotation with GeneMark-EP+ and AUGUSTUS supported by a protein database.
483 *NAR Genom Bioinform* 3: lqaa108.

484 Chakraborty M, Baldwin-Brown JG, Long AD, Emerson JJ. 2016. Contiguous and accurate de
485 novo assembly of metazoan genomes with modest long read coverage. *Nucleic Acids Res.*
486 44:e147.

487 Chakraborty M, Fry JD. 2015. Parallel functional changes in independent testis-specific
488 duplicates of Aldehyde dehydrogenase in *Drosophila*. *Mol. Biol. Evol.* 32:1029–1038.

489 Chin C-S, Alexander DH, Marks P, Klammer AA, Drake J, Heiner C, Clum A, Copeland A,
490 Huddleston J, Eichler EE, et al. 2013. Nonhybrid, finished microbial genome assemblies
491 from long-read SMRT sequencing data. *Nat. Methods* 10:563–569.

492 Cicconardi F, Lewis JJ, Martin SH, Reed RD, Danko CG, Montgomery SH. 2021. Chromosome
493 fusion affects genetic diversity and evolutionary turnover of functional loci, but
494 consistently depends on chromosome size. *Mol. Biol. Evol.* 38:4449–4462.

495 Connallon T, Clark AG. 2011. The resolution of sexual antagonism by gene duplication. *Genetics*
496 187:919–937.

497 Davey JW, Chouteau M, Barker SL, Maroja L, Baxter SW, Simpson F, Merrill RM, Joron M, Mallet
498 J, Dasmahapatra KK, et al. 2016. Major improvements to the *Heliconius melpomene*
499 genome assembly used to confirm 10 chromosome fusion events in 6 million years of
500 butterfly evolution. *G3* 6:695–708.

501 Dudchenko O, Batra SS, Omer AD, Nyquist SK, Hoeger M, Durand NC, Shamim MS, Machol I,
502 Lander ES, Aiden AP, et al. 2017. *De novo* assembly of the *Aedes aegypti* genome using Hi-
503 C yields chromosome-length scaffolds. *Science* 356:92–95.

504 Durand NC, Shamim MS, Machol I, Rao SSP, Huntley MH, Lander ES, Aiden EL. 2016. Juicer
505 provides a one-click system for analyzing loop-resolution Hi-C experiments. *Cell Syst* 3:95–
506 98.

507 Estrada C, Yildizhan S, Schulz S, Gilbert LE. 2010. Sex-specific chemical cues from immatures
508 facilitate the evolution of mate guarding in *Heliconius* butterflies. *Proceedings of the Royal
509 Society B: Biological Sciences* 277:407–413.

510 Finkbeiner SD, Briscoe AD. 2021. True UV color vision in a female butterfly with two UV opsins.
511 *J. Exp. Biol.* 224: jeb242802.

512 Flynn JM, Hubley R, Goubert C, Rosen J, Clark AG, Feschotte C, Smit AF. 2020. RepeatModeler2
513 for automated genomic discovery of transposable element families. *Proc. Natl. Acad. Sci.
514 U. S. A.* 117:9451–9457.

515 Fry JD. 2010. The genomic location of sexually antagonistic variation: some cautionary
516 comments. *Evolution* 64:1510–1516.

517 Guan D, McCarthy SA, Wood J, Howe K, Wang Y, Durbin R. 2020. Identifying and removing
518 haplotypic duplication in primary genome assemblies. *Bioinformatics* 36:2896–2898.

519 Guindon S, Dufayard J-F, Lefort V, Anisimova M, Hordijk W, Gascuel O. 2010. New algorithms
520 and methods to estimate maximum-likelihood phylogenies: assessing the performance of
521 PhyML 3.0. *Syst. Biol.* 59:307–321.

522 *Heliconius* Genome Consortium. 2012. Butterfly genome reveals promiscuous exchange of
523 mimicry adaptations among species. *Nature* 487:94–98.

524 Holt C, Yandell M. 2011. MAKER2: an annotation pipeline and genome-database management
525 tool for second-generation genome projects. *BMC Bioinformatics* 12:491.

526 Hsiao H-Y, Johnston RJ Jr, Jukam D, Vasilisuska D, Desplan C, Rister J. 2012. Dissection and
527 immunohistochemistry of larval, pupal and adult *Drosophila* retinas. *J. Vis. Exp.* 69:4347.

528 Hunt DM, Dulai KS, Cowing JA, Julliot C, Mollon JD, Bowmaker JK, Li WH, Hewett-Emmett D.
529 1998. Molecular evolution of trichromacy in primates. *Vision Res.* 38:3299–3306.

530 Jacobs GH. 1998. A perspective on color vision in platyrhine monkeys. *Vision Res.* 38:3307–
531 3313.

532 Jinek M, Chylinski K, Fonfara I, Hauer M, Doudna JA, Charpentier E. 2012. A programmable dual-
533 RNA-guided DNA endonuclease in adaptive bacterial immunity. *Science* 337:816–821.

534 Kim D, Paggi JM, Park C, Bennett C, Salzberg SL. 2019. Graph-based genome alignment and
535 genotyping with HISAT2 and HISAT-genotype. *Nat. Biotechnol.* 37:907–915.

536 Koren S, Walenz BP, Berlin K, Miller JR, Bergman NH, Phillippy AM. 2017. Canu: scalable and
537 accurate long-read assembly via adaptive k-mer weighting and repeat separation. *Genome*
538 *Res.* 27:722-736.

539 Kozak KM, Wahlberg N, Neild AFE, Dasmahapatra KK, Mallet J, Jiggins CD. 2015. Multilocus
540 species trees show the recent adaptive radiation of the mimetic *Heliconius* butterflies.
541 *Syst. Biol.* 64:505–524.

542 Langmead B, Salzberg SL. 2012. Fast gapped-read alignment with Bowtie 2. *Nat. Methods*
543 9:357–359.

544 Lefort V, Longueville J-E, Gascuel O. 2017. SMS: Smart model selection in PhyML. *Mol. Biol.*
545 *Evol.* 34:2422–2424.

546 Lewis JJ, van der Burg KRL, Mazo-Vargas A, Reed RD. 2016. ChIP-Seq-annotated *Heliconius erato*
547 genome highlights patterns of cis-Regulatory evolution in Lepidoptera. *Cell Rep.* 16:2855–
548 2863.

549 Lewis JJ, Cicconardi F, Martin SH, Reed RD, Danko CG, Montgomery SH. 2021. The *Dryas iulia*
550 genome supports multiple gains of a W chromosome from a B chromosome in butterflies.
551 *Genome Biol. Evol.* 13:evab128.

552 Liénard MA, Bernard GD, Allen A, Lassance J-M, Song S, Childers RR, Yu N, Ye D, Stephenson A,
553 Valencia-Montoya WA, et al. 2021. The evolution of red color vision is linked to
554 coordinated rhodopsin tuning in lycaenid butterflies. *Proc. Natl. Acad. Sci. U. S. A.*
555 118:e2008986118.

556 Long M, Emerson JJ. 2017. Meiotic sex chromosome inactivation: Compensation by gene traffic.
557 *Curr. Biol.* 27:R659–R661.

558 Manni M, Berkeley MR, Seppey M, Simão FA, Zdobnov EM. 2021. BUSCO update: Novel and
559 streamlined workflows along with broader and deeper phylogenetic coverage for scoring
560 of eukaryotic, prokaryotic, and viral genomes. *Mol. Biol. Evol.* 38:4647–4654.

561 Marçais G, Delcher AL, Phillippy AM, Coston R, Salzberg SL, Zimin A. 2018. MUMmer4: A fast
562 and versatile genome alignment system. *PLoS Comput. Biol.* 14:e1005944.

563 McCulloch KJ, Macias-Muñoz A, Mortazavi A, Briscoe AD. 2022. Multiple mechanisms of
564 photoreceptor spectral tuning in *Heliconius* butterflies. *Mol. Biol. Evol.* 39: msac067.

565 McCulloch KJ, Osorio D, Briscoe AD. 2016. Sexual dimorphism in the compound eye of
566 *Heliconius erato*: a nymphalid butterfly with at least five spectral classes of photoreceptor.
567 219:2377-87.

568 McCulloch KJ, Yuan F, Zhen Y, Aardema ML, Smith G, Llorente-Bousquets J, Andolfatto P,
569 Briscoe AD. 2017. Sexual dimorphism and retinal mosaic diversification following the
570 evolution of a violet receptor in butterflies. *Mol. Biol. Evol.* 34:2271–2284.

571 Mendoza-Cuenca L, Macías-Ordóñez R. 2005. Foraging polymorphism in *Heliconius charitonia*
572 (Lepidoptera: Nymphalidae): morphological constraints and behavioural compensation. *J.
573 Trop. Ecol.* 21:407–415.

574 Ogawa Y, Awata H, Wakakuwa M, Kinoshita M, Stavenga DG, Arikawa K. 2012. Coexpression of
575 three middle wavelength-absorbing visual pigments in sexually dimorphic photoreceptors
576 of the butterfly *Colias erate*. *J. Comp. Physiol.* 198:857–867.

577 Ou S, Su W, Liao Y, Chougule K, Agda JRA, Hellinga AJ, Lugo CSB, Elliott TA, Ware D, Peterson T,
578 et al. 2019. Benchmarking transposable element annotation methods for creation of a
579 streamlined, comprehensive pipeline. *Genome Biol.* 20:275.

580 Penz CM. 1999. Higher level phylogeny for the passion-vine butterflies (Nymphalidae,
581 Heliconiinae) based on early stage and adult morphology. *Zool. J. Linn. Soc.* 127:277–344.

582 Perry M, Kinoshita M, Saldi G, Huo L, Arikawa K, Desplan C. 2016. Molecular logic behind the
583 three-way stochastic choices that expand butterfly colour vision. *Nature* 535:280–284.

584 Perry MW, Desplan C. 2016. Love spots. *Curr. Biol.* 26:R484–R485.

585 Pertea M, Kim D, Pertea GM, Leek JT, Salzberg SL. 2016. Transcript-level expression analysis of
586 RNA-seq experiments with HISAT, StringTie and Ballgown. *Nat. Protoc.* 11:1650–1667.

587 Phillippy AM, Schatz MC, Pop M. 2008. Genome assembly forensics: finding the elusive mis-
588 assembly. *Genome Biol.* 9:R55.

589 Quinlan AR, Hall IM. 2010. BEDTools: a flexible suite of utilities for comparing genomic features.
590 *Bioinformatics* 26:841–842.

591 Rice WR. 1984. Sex chromosomes and the evolution of sexual dimorphism. *Evolution* 38:735–
592 742.

593 Roach MJ, Schmidt SA, Borneman AR. 2018. Purge Haplotigs: allelic contig reassignment for
594 third-gen diploid genome assemblies. *BMC Bioinformatics* 19:460.

595 Schindelin J, Arganda-Carreras I, Frise E, Kaynig V, Longair M, Pietzsch T, Preibisch S, Rueden C,
596 Saalfeld S, Schmid B, et al. 2012. Fiji: an open-source platform for biological-image
597 analysis. *Nat. Methods* 9:676–682.

598 Sison-Mangus MP, Bernard GD, Lampel J, Briscoe AD. 2006. Beauty in the eye of the beholder:
599 the two blue opsins of lycaenid butterflies and the opsin gene-driven evolution of sexually
600 dimorphic eyes. *J. Exp. Biol.* 209:3079–3090.

601 Solares EA, Tao Y, Long AD, Gaut BS. 2021. HapSolo: an optimization approach for removing
602 secondary haplotigs during diploid genome assembly and scaffolding. *BMC Bioinformatics*
603 22:9.

604 Turner JRG. 1976. Adaptive radiation and convergence in subdivisions of the butterfly genus
605 *Heliconius* (Lepidoptera: Nymphalidae). *Zool. J. Linn. Soc.* 58:297–308.

606 Turner JRG. 1978. Why male butterflies are non-mimetic: natural selection, sexual selection,
607 group selection, modification and sieving. *Biol. J. Linn. Soc. Lond.* 10:385–432.

608 Walker BJ, Abeel T, Shea T, Priest M, Abouelliel A, Sakthikumar S, Cuomo CA, Zeng Q, Wortman
609 J, Young SK, et al. 2014. Pilon: An integrated tool for comprehensive microbial variant
610 detection and genome assembly improvement. *PLoS One* 9:e112963.

611 Wood DE, Lu J, Langmead B. 2019. Improved metagenomic analysis with Kraken 2. *Genome*
612 *Biol.* 20:257.

613